

# Ultra-wideband Modelling of Optical Fibre Nonlinearity in Hybrid-amplified Links

Henrique Buglia

**Abstract**—Ultra-wideband (UWB) transmission using hybrid Raman amplifier technologies is a promising and cost-effective solution to meet the increasing demand for data traffic in optical fibre systems. The increased performance achieved by these amplifiers when compared to the lumped ones is an appealing solution to increase the total throughput of the transmission link. However, accurate and real-time system performance estimation is required. This work presents the first fully analytical model to estimate the performance of the optical system in the presence of hybrid Raman amplifiers and inter-channel stimulated Raman scattering (ISRS) effect. The model accounts for the fibre nonlinear interference (NLI), amplified spontaneous emission (ASE) generated by Raman amplification (RA) and transceiver (TRX) noise. It also supports any RA setup, such as an arbitrary number of forward (FW) and/or backward (BW) pumps, wavelength-dependent parameters, variable modulation formats, per-channel launch powers and channel bandwidth. The performance of an 80 km multi-span 13 THz transmission system is assessed and capacity-maximising hybrid Raman amplifiers are designed based on a particle swarm optimisation (PSO) algorithm, where the analytical nonlinear model is used to achieve real-time optimisation. An extensive theoretical investigation for different systems configurations ranging from short to metro, long-haul and trans-Atlantic is described, demonstrating the trade-off between the different sources of noise and amplifier technologies.

**Index Terms**—Ultra-wideband transmission, Raman amplification, lumped amplification, hybrid amplification, S+C+L band transmission, closed-form approximation, Gaussian noise model, nonlinear interference, nonlinear distortion, optical fibre communications, inter-channel stimulated Raman scattering

## I. INTRODUCTION

**M**ORE than 35 years have passed since the publication of the first experimental demonstration of the erbium-doped fibre amplifier (EDFA) [1]. The possibility of simultaneously amplifying channels within approximately 4 THz of optical bandwidth, which came to be known as the C- (conventional, 1530-1565 nm)-band, an order of magnitude greater than the entire radio spectrum, offered what seemed an inexhaustible communication resource for the future and enabled wavelength division multiplexing (WDM). However, 35 years on, the exponential growth of bandwidth-hungry internet services including high-definition video streaming, cloud computing, artificial intelligence, Big Data and the Internet of Things urgently need new advances in optical data

transmission technologies to enable ultra-high throughput with minimal latencies. This applies to all types of networks, from metro, access networks, and inter-data centre links through to wide-area terrestrial and ultra-long haul transoceanic systems.

To cope with this, new technologies such as UWB transmission and space-division multiplexing (SDM) have been widely explored in recent years [2]–[4]. For UWB transmission systems, exploring the low-loss wavelength window of a silica-based optical fibre, as shown in Fig. 2, requires the utilisation of new amplifier technologies in addition to EDFAs, operating beyond C+L bands. These include thulium-doped fibre amplifiers (TDFA), semiconductor optical amplifiers (SOA) and RA [5]–[19], which have been used over the past few years to achieve milestones of data throughput in single-mode fibres (SMF) over different distances, as shown in Fig. 1.

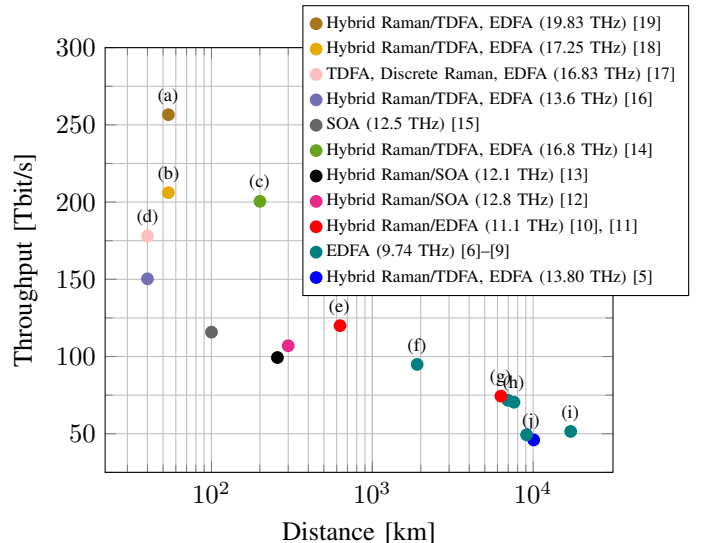


Fig. 1. Record data throughput versus distance for SMF, not including spectral gaps between amplifier gain bandwidths, with the most recent and key results highlighted in the figure: (a) [19], (b) [18], (c) [14], (d) [17], (e) [10], (f) [4], (g) [11], (h) [7], (i) [9], and (j) [19].

Fig. 1 also shows that all the most recent works, i.e., (a)–(i), achieve records transmission using a combination of lumped and RA, also known as hybrid-amplification technology. Such a strategy explores the better ASE-noise performance of RA when compared to the lumped amplifiers (LA), and thus, enables an increase in the achievable total throughput of the deployed systems [20]. RA can be divided into two types, namely distributed RA and discrete RA. For the former, the pumps are injected into the transmission fibre, while for the

This work is funded by the EPSRC studentship EP/T517793/1 and the Microsoft 'Optics for the Cloud' Alliance.

The author is with the Optical Networks Group, University College London, Department of Electronic and Electrical Engineering, Roberts Building, Torrington Place, London WC1E 7JE, U.K (e-mail: henrique.buglia.20@ucl.ac.uk).

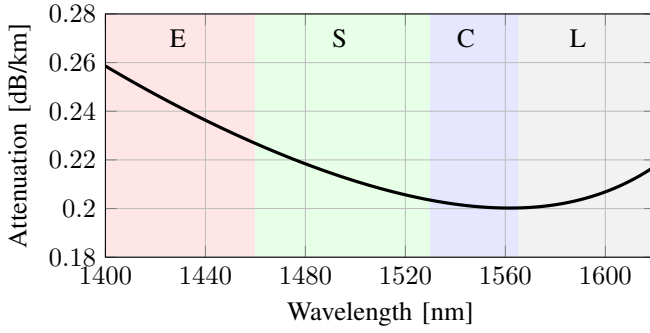


Fig. 2. Attenuation coefficient of an ITU-T G652.D fibre.

latter a separate fibre is used as the amplification stage. In both cases, the pumps interact with the signal to provide the desired signal amplification.

Together with new amplifier technologies, the necessity of maximising the system throughput in optical networks requires the development of real-time models. This is a key step to introduce intelligence in the network, delivering capacity when and where it is needed [21], [22]. Additionally, it also enables online network optimisation routines, maximisation of the network efficiency, rapid system design, and virtualisation of the physical layer.

Real-time nonlinear UWB models have been developed via closed-form expressions of the Gaussian noise (GN) model and its extensions [23]–[25]. Using this model in real-time requires the development of closed-form expressions to overcome the time-consuming computation of the integral expressions involved in it. Moreover, this model offers a simple way of estimating the fibre NLI by treating it as additive Gaussian noise. Numerous closed-form expressions have been proposed to date [26]. Of interest for UWB transmission systems are closed-form expressions for the GN model in the presence of ISRS effect [25], namely ISRS GN model. Closed-form expressions of this model were derived in [27]–[35].

Most of the aforementioned works were developed for LA technologies, limiting the validity of the models to this amplification scheme. As mentioned, current high-capacity optical fibre systems require nonlinear models capable of accounting also for RA, enabling the assessment of hybrid-amplified optical links. This later enables an increase in the data throughput of the deployed optical systems. More importantly, these models need to be general and valid for all the RA setups. The works published in [31], [32] enable RA amplification, however, it is limited to FW pumping amplification schemes and, were applied only over C-band systems. The same happens in [36], which is only valid for 2<sup>nd</sup> order Raman amplification (RA), i.e., the utilisation of two or fewer pumps over C-band systems.

The first nonlinear model capable of accurately estimating UWB hybrid-amplified links for any system setup was developed in the works [37]–[39]. This general characteristic involves the inclusion of the NLI noise generated by RA together with ISRS effect and the flexibility of using this model for any RA setup, such as FW and/or BW pumping amplification schemes, arbitrary-order RA, i.e., an arbitrary

number of pumps, and arbitrary constellations designs, i.e., Gaussian [38], shaped or square [39] modulation formats. These characteristics were enabled by deriving for the first time a semi-analytical solution to model the signal profile in the presence of RA and ISRS [38].

In this work, we extensively model the aspects of hybrid-amplified transmission systems. In particular, we consider a baseline S-,C-,L- band system, corresponding to an optical transmission bandwidth of 13 THz (105 nm) and we design and model a transmission using hybrid amplification, where launch power, FW and BW pumps are optimised to achieve the maximum system throughput in a distributed Raman pumping configuration where the pumps are injected in the transmission fibre. The maximisation is done using the capacity ( $C$ ) Shannon’s upper-bound formula  $C = \frac{1}{2} \log_2(1 + \text{SNR})$ , with SNR being the total signal-to-noise ratio, and the NLI noise calculated using the model in [38]. To calculate the total SNR, we also include ASE noise generated by RA in the model developed in [38], presenting for the first time a complete analytical model to estimate the system performance in hybrid amplification scenarios. Furthermore, we present a complete characterisation of the optimised amplifier, such as its gain and how the ISRS affects its optimal design. Moreover, the system performance is also presented, where we separate out each one of the noise sources contributions to the total SNR, analysing the trade-off and relations of these sources with the capacity-achieving amplifier design. Finally, a comparison of this optimised system with the one operating over a full LA scheme is carried out, enabling us to access and show the different noise source interactions for each one of the systems, and the full benefits of using RA schemes.

This paper is divided as follows, Sec II describes the ISRS effect and RA, and how it affects the NLI noise of the system. Sec. III presents the nonlinear model used to compute and estimate all the results of this paper. Sec. IV describes the transmission system setup. Sec V describes the pump and launch power optimisation algorithm used for the capacity-achieving hybrid amplifier design, which maximises the transmission system throughput. Sec. VI gives the optimised amplifier characterisation in terms of its on-off gain, power profile evolution, and also analyses the impact of the ISRS effect on the designed amplifier. Sec. VII presents the noise contributions of each one of the noise sources and the total system performance based on the total SNR. Sec. VIII compares the optimised hybrid-amplifier system performance, with that of a system designed using a full lumped amplifier. Finally, Sec. IX concludes this work.

## II. INTER-CHANNEL STIMULATED RAMAN SCATTERING AND RAMAN AMPLIFICATION

This section describes the effects of ISRS and RA, which are jointly included in the closed-form expression derived in [38]. The inclusion of these effects is essential for modelling any ultra-wideband system that uses RA technologies.

As it is well known, in the framework of the GN model with no NLI interference compensation technique, such as digital-back propagation, the NLI interference is proportional

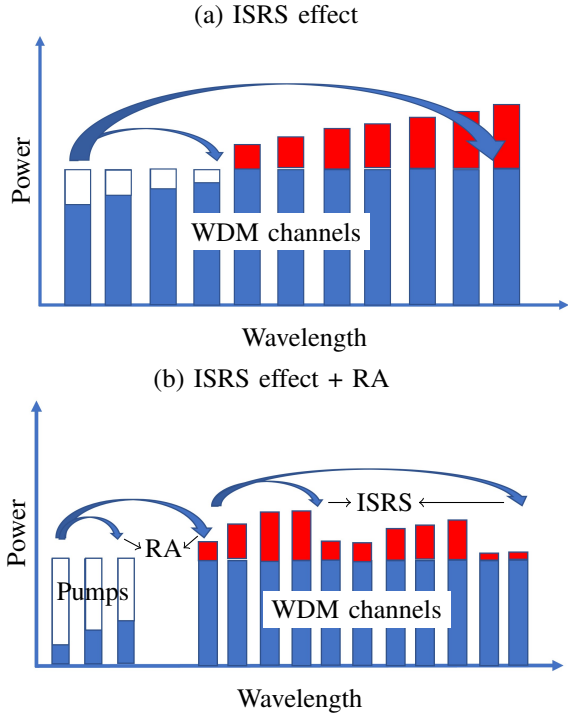


Fig. 3. Illustration of the ISRS effect (a) only and (b) jointly with RA.

to the cube of the optical power injected into the fibre. This being said, any nonlinear effect that alters the channel power distribution, will also alter the NLI noise distribution in each channel. This is the case of the ISRS effect and the RA.

Due to the ISRS effect, lower-wavelength channels transfer power to higher-wavelength channels, as depicted in Fig. 3.(a). This power transfer increases the NLI noise for channels located at higher wavelengths, due to their increased power levels. Similarly, an opposite effect happens for the lower-wavelength channels. This does not mean that the total NLI is always higher for higher-wavelength channels, as the effect of dispersion and attenuation must also be taken into account in the NLI noise estimation.

The amount of power that is transferred from one channel to another follows the Raman gain spectrum shown in Fig. 4, and it depends on the frequency separation of the channels, achieving a maximum at around a 13.5 THz frequency separation. For lumped-only amplified systems, closed-form expressions of the GN model were previously derived - with the inclusion of ISRS - in the works [27]–[30], [33]–[35].

RA has a similar effect when compared to the ISRS effect. It also produces a power transfer, but from pumps to the channels. When acting jointly with the ISRS effect, this transfer of power occurs in all directions, i.e., from pumps to pumps, pumps to channels and channels to channels, as depicted in Fig. 3.(b). It also follows the Raman gain spectrum in Fig. 4 and in this case, the amount of power transferred from the pumps to each channel will be dependent on the pump wavelengths and their powers. The pumps are usually chosen to give gains in specific portions of the signal spectrum. This selection is done by placing the pumps at an approximate

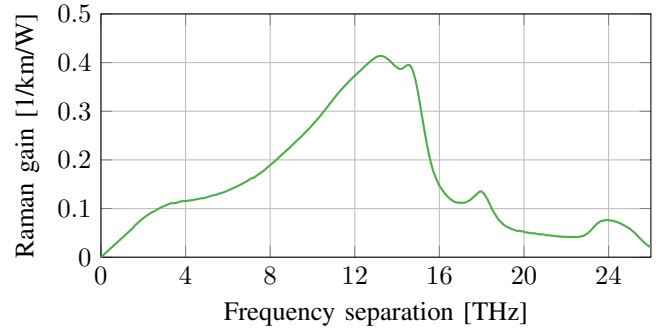


Fig. 4. Raman gain spectrum of an ITU-T G652.D fibre.

distance of 13.5 THz from the desired regions of the signal spectrum to be amplified.

Due to increased power which is transferred from the pumps to the WDM spectra, the amount of NLI noise present in the signal when compared to the LA case is higher for Raman-amplified links. Despite this disadvantage, Raman-amplified links still generally perform better than LA because of the reduced levels of ASE noise. This is shown in detail in Secs. VII and VIII. For RA systems, closed-form expressions were derived in [31], [32], [36]–[38]. Remarkably are the closed-form expressions in [37]–[39], as they are valid for all scenarios of Raman-amplified systems, such as an arbitrary number of FW and/or BW pumps, wavelength-dependent parameters, variable modulation formats, per-channel launch powers and channel bandwidth.

The ISRS effect and RA also affect the optimum launch power distribution and the pump wavelengths and powers which maximises the system throughput. This is because the NLI and ASE noises depend on the per-channel launch power and on the pump wavelength and power allocation. Moreover, this multidimensional-optimisation problem is non-convex [40]. For LA in the presence of ISRS, this fact was discussed and analysed using global optimisation algorithms such as evolutionary algorithms (EA) [41], [42], PSO [3], [4], artificial neural network (ANN) [43] and faster but sub-optimal strategies [44]. Most importantly, the speed of these algorithms has been improved through analytical closed-form expressions [45], [46] or even ANN [47], [48] models that estimate the NLI in the presence of ISRS. For Raman-amplified links, however, this topic has been hardly explored [32] due to the very recent development of closed-form expressions fully able to account for all RA setups [37]–[39]. This topic is explored throughout this paper in Sec.V.

### III. NONLINEAR MODEL

This section presents the analytical nonlinear model used to derive the results of this paper. The coupled signal power profile evolution equations are first introduced for each amplification scheme (LA and RA), followed by the equations characterising the ASE and NLI noises.

#### A. The received SNR

To estimate the total SNR, the impairments arising from the TRX, inline optical amplifiers to compensate for the fibre

loss, and fibre nonlinearities are taken into account as additive terms, such that each source of impairment is statistically independent of one another. The received total SNR for the  $i^{\text{th}}$  WDM channel after the  $n^{\text{th}}$  amplifier is then given by

$$\text{SNR}_i^{-1} \approx \text{SNR}_{\text{TRX}}^{-1} + \text{SNR}_{\text{ASE}}^{-1} + \text{SNR}_{\text{NLI}}^{-1} = \left( \frac{P_i}{\kappa_i P_i + P_{\text{ASE}_i} + \eta_n(f_i) P_i^3} \right)^{-1}, \quad (1)$$

where  $\text{SNR}_{\text{TRX}}$ ,  $\text{SNR}_{\text{ASE}}$  and  $\text{SNR}_{\text{NLI}}$  are the SNR from the transceiver subsystem or back-to-back implementation penalty, the ASE from the optical amplifier used to compensate for the fibre loss and the accumulated NLI, respectively.  $n$  is the number of spans,  $i$  is the channel under consideration,  $P_i$  is its launch power,  $\kappa_i = 1/\text{SNR}_{\text{TRX}_i}$ ,  $P_{\text{ASE}_i}$  is the ASE noise power, and  $P_{\text{NLI}_i} = \eta_n(f_i) P_i^3$  is the NLI noise power after  $n$  spans. Eq. (1) assumes that the input power is completely recovered after the  $n^{\text{th}}$  amplifier. Throughout the remainder of this paper to simplify the analysis, we will consider an ideal TRX, such that  $\text{SNR}_{\text{TRX}} \rightarrow \infty$ .

### B. Signal power profile evolution

Let  $\rho(z, f_i) = \frac{P_i(z)}{P_i(0)}$  be the normalised signal power profile evolution along the optical fibre. For distributed Raman amplifiers, the evolution of the channel of interest (COI) power along the fibre distance is written as

$$\begin{aligned} \pm \frac{\partial P_i}{\partial z} = & - \sum_{k=i+1}^{N_{\text{ch}}} \frac{f_k}{f_i} g(|\Delta f|) (P_k + P_{\text{ASE},k}) P_i - \\ & - \sum_{p:f_i > f_p} \frac{f_p}{f_i} g(|\Delta f|) (P_p + P_{\text{ASE},p}) P_i + \\ & + \sum_{k=1}^{i-1} g(|\Delta f|) (P_k + P_{\text{ASE},k}) P_i + \\ & + \sum_{p:f_i < f_p} g(|\Delta f|) (P_p + P_{\text{ASE},p}) P_i - \alpha_i P_i, \end{aligned} \quad (2)$$

where,  $P_i$ ,  $f_i$  are the power and frequency of the COI,  $P_k$ ,  $f_k$  are the power and frequency of the remaining WDM channels,  $P_p$ ,  $f_p$  are the power and the frequency of the pumps,  $g_r(|\Delta f|)$  is the polarisation averaged, normalized (by the effective core area  $A_{\text{eff}}$ ) Raman gain spectrum for a frequency separation  $|\Delta f| = |f_i - f_k|$ ,  $j = k, p$  and  $\alpha_i$  is the frequency-dependent attenuation coefficient.  $P_{\text{ASE},i}$ ,  $P_{\text{ASE},k}$  and  $P_{\text{ASE},p}$  are the ASE noise respectively in the COI, channel  $k$  and pump  $p$ . The symbol  $\pm$  represents the pump under consideration, i.e.,  $+$  for FW-pump and  $-$  for BW-pump configurations. The pump and remaining channel equations are obtained by replacing  $i = p, k$  in Eq. (2). Note that, this equation is solved for each span, where the accumulated ASE noise at the end of each span is used as the initial condition for the following span.

In the right-hand side of Eq. (2), the first and third terms represent respectively the COI power loss and gain due to ISRS effect, and the second and fourth terms represent the COI loss and gain due to RA. Usually, pumps are placed on the right-hand side of the WDM frequency spectrum (and not in the middle), such that the second term is zero. Finally, the last term is the COI power loss due to wavelength-dependent

fibre attenuation. Note that, both the RA and the ISRS effect are influenced by the ASE noise. The impact of the ASE noise in Eq. (2) is computed in Sec.VII.

In the case of LA, where no pumps are present in the signal spectrum, it is shown to be a good approximation to also neglect the ASE coupled noise and consider only the fibre loss and the ISRS effect, such that, Eq. (2) reduces to

$$\begin{aligned} \frac{\partial P_i}{\partial z} = & - \sum_{k=i+1}^{N_{\text{ch}}} \frac{f_k}{f_i} g(|\Delta f|) P_k P_i + \\ & + \sum_{k=1}^{i-1} g(|\Delta f|) P_k P_i - \alpha_i P_i. \end{aligned} \quad (3)$$

### C. ASE noise

For Raman-amplified links, the ASE noise power at the frequency of the  $i^{\text{th}}$  channel,  $P_{\text{ASE}_i}$ , is calculated as the solution of the following coupled differential equations:

$$\begin{aligned} \frac{\partial P_{\text{ASE}_i}}{\partial z} = & - \sum_{k=i+1}^{N_{\text{ch}}} \frac{f_k}{f_i} g(|\Delta f|) (P_k + P_{\text{ASE},k}) (P_{\text{ASE}_i} + 2hn_{\text{sp}} B_i f_i) - \\ & - \sum_{p:f_i > f_p} \frac{f_p}{f_i} g(|\Delta f|) (P_p + P_{\text{ASE},p}) (P_{\text{ASE}_i} + 2hn_{\text{sp}} B_i f_i) + \\ & + \sum_{k=1}^{i-1} g(|\Delta f|) (P_k + P_{\text{ASE},k}) (P_{\text{ASE}_i} + 2hn_{\text{sp}} B_i f_i) + \\ & + \sum_{p:f_i < f_p} g(|\Delta f|) (P_p + P_{\text{ASE},p}) (P_{\text{ASE}_i} + 2hn_{\text{sp}} B_i f_i) - \alpha_i P_{\text{ASE}_i}, \end{aligned} \quad (4)$$

where  $P_{\text{ASE},k}$  and  $P_{\text{ASE},p}$  are respectively the ASE noise from the channel  $k$  and the pump  $p$ .  $B_i$  is the bandwidth of the COI. The ASE equations for the remaining WDM channels and pumps are obtained by setting  $i = k$  and  $i = p$  respectively. Eq. (4) is solved for each one of the spans with initial conditions at the beginning of the first span as  $P_{\text{ASE}_i} = P_{\text{ASE},k} = P_{\text{ASE},p} = 0$ .

The spontaneous emission factor  $n_{\text{sp}}$  is given by

$$n_{\text{sp}} = \frac{1}{1 - e^{-\frac{h\Delta f}{k_B T}}}, \quad (5)$$

where  $h$  is Planck constant,  $T$  is the temperature of the system and  $k_B$  is Boltzmann's constant.

For lumped amplifiers, the ASE noise in the channel  $i$  after one span,  $P_{\text{ASE}_i}$  is well accepted to be approximated and given by

$$P_{\text{ASE}_i} = 2(G_i - 1)n_{\text{sp}} h f_i B_i, \quad (6)$$

where  $n_{\text{sp}} \approx \frac{\text{NF}}{2}$ , with NF the amplifier noise figure, and  $G_i = P_i(L)/P_i(0)$  is the amplifier gain at the frequency of the  $i^{\text{th}}$  channel, where  $P_i(0)$  and  $P_i(L)$  are the powers of channel  $i$  at the input and output of the considered span, respectively.

### D. NLI noise

For any amplification technique, the NLI noise is given by  $P_{\text{NLI}_i} = \eta_n(f_i) P_i^3$ . The nonlinear coefficient  $\eta_n(f_i)$  can be approximated as

$$\eta_n(f_i) \approx \sum_{j=1}^n \left[ \frac{P_{i,j}}{P_i} \right]^2 \cdot [\eta_{\text{SPM}_j}(f_i) n^\epsilon + \eta_{\text{XPM}_j}(f_i)], \quad (7)$$

where  $\eta_{\text{SPM}_j}(f_i)$  is the self-phase modulation (SPM) contribution and  $\eta_{\text{XPM}_j}(f_i)$  is the total cross-phase modulation (XPM) contribution to the NLI both generated in the  $j^{\text{th}}$  span.  $P_{i,j}$  is the power of channel  $i$  launched into the  $j^{\text{th}}$  span,  $\epsilon$  is the coherent factor [23, Eq. (22)]. In Eq. (7), the four-wave mixing (FWM) contributions to the NLI are neglected, the SPM is assumed to accumulate coherently along the fibre spans, while the XPM is assumed to accumulate incoherently - the accuracy of these assumptions was validated in [28]. For notation convenience, the  $j$  dependence of the SPM and XPM contribution is suppressed throughout this paper.

The XPM contribution ( $\eta_{\text{XPM}}(f_i)$ ) in Eq. (7) is obtained by summing over all COI-interfering pairs present in the transmitted signal, i.e.,

$$\eta_{\text{XPM}}(f_i) = \sum_{k=1, k \neq i}^{N_{\text{ch}}} \eta_{\text{XPM}}^{(k)}(f_i), \quad (8)$$

where  $N_{\text{ch}}$  is the number of WDM channels and  $\eta_{\text{XPM}}^{(k)}(f_i)$  is the XPM contribution of a single interfering channel  $k$  on channel  $i$ . In Eq. (8), the XPM contributions from the COI-pump pairs are neglected, i.e.,  $\sum_{p=1, p \neq i}^{N_p} \eta_{\text{XPM}}^{(p)}(f_i) = 0$ , where  $N_p$  is the number of pumps (if any). This was shown to be a reasonable assumption when pumps are far away from the WDM spectra [49].

For Raman-amplified links, analytical expressions for the XPM and SPM NLI contributions of Eq. (7) were previously derived in [38], respectively as

$$\begin{aligned} \eta_{\text{XPM}}^{(k)}(f_i) &= \frac{32}{27} \frac{\gamma^2}{B_k} \left( \frac{P_k}{P_i} \right)^2 \sum_{\substack{0 \leq l_1 + l_2 \leq 1 \\ 0 \leq l'_1 + l'_2 \leq 1}} \Upsilon_k \Upsilon'_k \frac{1}{\phi_{i,k}(\alpha_{l,k} + \alpha'_{l,k})} \times \\ &\times \left\{ 2(\kappa_{f,k} \kappa'_{f,k} + \kappa_{b,k} \kappa'_{b,k}) \left[ \text{atan} \left( \frac{\phi_{i,k} B_i}{2\alpha_{l,k}} \right) + \text{atan} \left( \frac{\phi_{i,k} B_i}{2\alpha'_{l,k}} \right) \right] + \right. \\ &+ \pi \left[ -(\kappa_{f,k} \kappa'_{b,k} + \kappa_{b,k} \kappa'_{f,k}) \left( \text{sign} \left( \frac{\alpha_{l,k}}{\phi_{i,k}} \right) e^{-|\alpha_{l,k} L|} + \right. \right. \\ &+ \left. \left. \text{sign} \left( \frac{\alpha'_{l,k}}{\phi_{i,k}} \right) e^{-|\alpha'_{l,k} L|} \right) + (\kappa_{f,k} \kappa'_{b,k} - \kappa_{b,k} \kappa'_{f,k}) \times \right. \\ &\left. \left. \times \left( \text{sign}(-\phi_{i,k}) e^{-|\alpha_{l,k} L|} + \text{sign}(\phi_{i,k}) e^{-|\alpha'_{l,k} L|} \right) \right] \right\} \end{aligned} \quad (9)$$

and

$$\begin{aligned} \eta_{\text{SPM}}(f_i) &= \frac{16}{27} \frac{\gamma^2}{B_i^2} \sum_{\substack{0 \leq l_1 + l_2 \leq 1 \\ 0 \leq l'_1 + l'_2 \leq 1}} \Upsilon_i \Upsilon'_i \frac{\pi}{\phi_i(\alpha_{l,i} + \alpha'_{l,i})} \times \\ &\times \left\{ 2(\kappa_{f,i} \kappa'_{f,i} + \kappa_{b,i} \kappa'_{b,i}) \left[ \text{asinh} \left( \frac{3\phi_i B_i^2}{8\pi\alpha_{l,i}} \right) + \text{asinh} \left( \frac{3\phi_i B_i^2}{8\pi\alpha'_{l,i}} \right) \right] + \right. \\ &+ 4 \ln \left( \sqrt{\frac{\phi_i L}{2\pi}} B_i \right) \left[ -(\kappa_{f,i} \kappa'_{b,i} + \kappa_{b,i} \kappa'_{f,i}) \left( \text{sign} \left( \frac{\alpha_{l,i}}{\phi_i} \right) e^{-|\alpha_{l,i} L|} + \right. \right. \\ &+ \left. \left. \text{sign} \left( \frac{\alpha'_{l,i}}{\phi_i} \right) e^{-|\alpha'_{l,i} L|} \right) + (\kappa_{f,i} \kappa'_{b,i} - \kappa_{b,i} \kappa'_{f,i}) \times \right. \\ &\left. \left. \times \left( \text{sign}(-\phi_i) e^{-|\alpha_{l,i} L|} \text{sign}(\phi_i) e^{-|\alpha'_{l,i} L|} \right) \right] \right\}, \end{aligned} \quad (10)$$

where

$$\begin{aligned} \phi_i &= -4\pi^2 (\beta_2 + 2\pi\beta_3 f_i), \\ \phi_{i,k} &= -4\pi^2 (f_k - f_i) [\beta_2 + \pi\beta_3 (f_i + f_k)], \end{aligned}$$

$$\begin{aligned} T_{f,i} &= -\frac{P_f C_{f,i}(f_i - \hat{f})}{\alpha_{f,i}}, & T_i &= 1 + T_{f,i} - T_{b,i} e^{-\alpha_{b,i} L}, \\ T_{b,i} &= -\frac{P_b C_{b,i}(f_i - \hat{f})}{\alpha_{b,i}}, & \alpha_{l,i} &= \alpha_i + l_1 \alpha_{f,i} - l_2 \alpha_{b,i}, \\ & & \kappa_{f,i} &= e^{-(\alpha_i + l_1 \alpha_{f,i}) L}, \\ & & \kappa_{b,i} &= e^{-l_2 \alpha_{b,i} L}, \end{aligned}$$

$$\Upsilon_i = T_i \left( \frac{-T_{f,i}}{T_i} \right)^{l_1} \left( \frac{T_{b,i}}{T_i} \right)^{l_2},$$

$\beta_2$  is the group velocity dispersion (GVD) parameter,  $\beta_3$  is the linear slope of the GVD parameter,  $\gamma$  is the nonlinear parameter and  $B_k$  is the bandwidth of the channel  $k$ . The coefficients  $\Upsilon'_i$ ,  $\alpha'_{l,i}$ ,  $\kappa'_{f,i}$  and  $\kappa'_{b,i}$  are respectively the same ones as  $\Upsilon_i$ ,  $\alpha_{l,i}$ ,  $\kappa_{f,i}$  and  $\kappa_{b,i}$  but with the indices  $l_1$  and  $l_2$  replaced by  $l'_1$  and  $l'_2$ .  $L$  is the fibre length,  $P_f$  is the sum of the channel together with the FW pump powers and  $P_b$  is the sum of the BW pump powers.  $\hat{f}$  is the average frequency of the pumps.  $\alpha_i$ ,  $\alpha_{f,i}$  and  $\alpha_{b,i}$  are fibre attenuation coefficients,  $C_{f,i}$  and  $C_{b,i}$  is the slope of a linear regression of the normalised Raman gain spectrum.

The determination of the channel-dependent coefficients  $\alpha_i$ ,  $\alpha_{f,i}$ ,  $\alpha_{b,i}$ ,  $C_{f,i}$  and  $C_{b,i}$  follows the strategy described in [38], i.e., the following analytical function is used:

$$\rho(z, f_i) = e^{-\alpha_i z} [1 - (C_{f,i} P_f L_{\text{eff}} + C_{b,i} P_b \tilde{L}_{\text{eff}})(f_i - \hat{f})], \quad (11)$$

where

$$\begin{aligned} L_{\text{eff}}(z) &= (1 - e^{-\alpha_{f,i} z}) / \alpha_{f,i}, \\ \tilde{L}_{\text{eff}}(z) &= (e^{-\alpha_{b,i}(L-z)} - e^{-\alpha_{b,i} L}) / \alpha_{b,i}. \end{aligned}$$

The coefficients  $\alpha_i$ ,  $\alpha_{f,i}$ ,  $\alpha_{b,i}$ ,  $C_{f,i}$  and  $C_{b,i}$  are then optimised using nonlinear least-squares fitting, such that the values obtained for the 5 coefficients in Eq. (11), correctly reproduce the power profile obtained from the Raman differential equations in the presence of RA, i.e., from Eq. (2).

The parameters  $\alpha_i$ ,  $C_{f,i}$ ,  $C_{b,i}$ ,  $\alpha_{f,i}$ , and  $\alpha_{b,i}$  can be interpreted as modelling respectively the fibre loss, the gain/loss due to FW-RA and BW-RA together with ISRS and how fast the channel gain/loss due to the FW-RA and BW-RA together with ISRS extinguishes along the fibre. This fitting optimisation procedure enables the utilisation of Eqs. (9) and Eq. (10) in any simulation scenarios, such as any number of pumps, launch power profiles and channel bandwidths. Additionally, the formula is also valid for links made of different span setups - in that case, all the fibre parameters and per-channel launch power depend not only on the channel  $i$  but also on the span  $j$ .

For LA, more simplified equations for the SPM and XPM NLI contributions can be used. These equations were published in [28] as Eqs. (10) and (11).

#### IV. TRANSMISSION SYSTEM SETUP

This section describes the transmission system we use for all the analyses in this paper. It consists of a WDM signal with  $N_{\text{ch}}=131$  channels spaced by 100 GHz and centred at 1550 nm. Each channel was modulated at the symbol rate of 96 GBd, resulting in a total bandwidth of 13 THz (105 nm), ranging from 1500 nm to 1605 nm, corresponding to the transmission over the S- (1470 nm - 1520nm), C- (1530 nm - 1565nm) and L- (1570 nm - 1615nm) bands. Spectral gaps of 10 nm and 5 nm are considered, respectively between the S/C and C/L band. The NF of each lumped amplifier placed at the end of each span is 6 dB, 5 dB, and 6 dB in the S-, C- and L- band, respectively. For simplicity, we consider Gaussian constellations, such that we can directly apply the model in Sec. III, however, other types of constellations could be easily considered by using the additional NLI correction term in [39].

A generic SMF corresponding to an ITU-T G652.D fibre with attenuation profile and the Raman gain spectrum shown respectively in Figs. 2 and 4 is considered. The nonlinear parameter, effective core area ( $A_{\text{eff}}$ ), dispersion, and dispersion slope are assumed to be  $\gamma = 1.16 \text{ W}^{-1}\text{km}^{-1}$ ,  $A_{\text{eff}} = 81 \mu\text{m}^2$ ,  $D = 16.5 \text{ ps nm}^{-1}\text{km}^{-1}$ ,  $S = 0.09 \text{ ps nm}^{-2}\text{km}^{-1}$ , respectively. An ideal TRX subsystem is also assumed as mentioned in Sec. III.

A transmission link made of multiple spans of 80 km is considered. Simulations are carried out for 1, 10 and 100 spans in order to simulate distances ranging from short to metro, long-haul and trans-Atlantic transmission systems. A hybrid amplification scheme made of a distributed Raman amplifier followed by an LA is considered. The LA at the end of each span is assumed to be ideal, such that the transmitted power is completely recovered at the end of each span. To that end, after distributed RA, the lumped gain at the end of each span is assumed to be controlled to the target value by using adaptive spectral equalisation and amplifier dynamic gain control devices. A spectrally uniform launch power profile is considered, which is optimised together with the pumps to maximise the system throughput (see Sec. V). A generic launch power profile could also be considered, however for simplicity and computational time reduction, we chose to operate with a spectrally uniform one as explained in Sec. V.

#### V. THROUGHPUT MAXIMISATION FOR HYBRID-AMPLIFIED TRANSMISSION

This section describes the throughput maximisation strategy used in this paper to maximise the system performance given by Eq. (1). Due to the RA and the ISRS effect, the relation between system performance, pumps' powers and launch power is nonlinear, leading to a  $N_{\text{ch}} + N_{\text{p}}$ -dimensional non-convex optimisation problem [40]. To solve this problem, numerical optimisation algorithms are required.

The goal of this optimisation is to find the optimum pump wavelengths and powers together with the optimum channel launch power, which maximises the total throughput for the hybrid RA transmission system considered in Sec. IV. The

total throughput is bounded above by the AWGN channel capacity:

$$C_{\text{Total}} = \sum_{i=1}^{N_{\text{ch}}} C_i = \sum_{i=1}^{N_{\text{ch}}} 2 \cdot \log_2(1 + \text{SNR}_i), \quad (12)$$

where  $\text{SNR}_i$  is obtained from Eq. (1) and  $C_i$  is the AWGN capacity for the  $i^{\text{th}}$  channel. Eq. (12) is the cost function considered in the optimisation, where  $\text{SNR}_i$  is calculated from Eq. (1). Note that, the ASE generated by the distributed Raman stage and by the lumped amplifier are calculated using Eqs. (4) and (6), respectively.

The numerical optimisation algorithm chosen to find a local maximum of (12) is the PSO [50]. The PSO is efficient in exploring the  $N_{\text{ch}} + N_{\text{p}}$ -dimensional space leading to the surroundings of a good local optimal solution in this  $N_{\text{ch}} + N_{\text{p}}$ -dimensional surface. For this algorithm, we use the Matlab PSO function provided by the global optimisation toolbox.

In order to reduce the complexity of this algorithm, we chose to optimise a spectrally uniform launch power profile, such that each channel carries the same launch power. This enables the reduction of the optimisation space from  $N_{\text{ch}} + N_{\text{p}}$  to  $N_{\text{p}} + 1$ . For this optimisation, transmission over a single span is considered, and the solution of this optimisation is used for pumping all the remaining amplifiers in the multi-span transmission scenarios (see Sec. IV). This approach is not optimum as the optimum amplifier design changes slightly for each span. This is because the NLI and the ASE noises generated in each span accumulate in a nonlinear manner. However, this non-optimal choice reduces the complexity of the optimisation algorithm as Eqs. (2) and (4) are solved for a single span only. Moreover, in terms of NLI noise, it was shown in [4] that assuming this optimisation for a single span to be also optimum for more spans does not deviate a lot from the true optimum solution for more than 1 span.

We consider two different hybrid-amplification simulation scenarios, each one using the following distributed setup: FW-RA and BW-RA. Over the E- and S-band we place 16 pumps spaced from 0.5 THz apart and let the algorithm find the best power allocation for these pumps, i.e., the allocation which maximises Eq. (12), considering an idea lumped amplifier at end of the span to give the remaining signal gain in order to completely recover the transmitted power. The highest-wavelength pump was chosen to be 2 THz away from the lowest-wavelength channel, such that we can neglect the XPM-induced products from pumps falling into the WDM spectrum [49].

For both cases, 17 variables are then optimised, whereas in each case 1 variable is the spectrally uniform launch power and the remaining are the pumps. For the PSO algorithm, the number of particles is chosen to be the same as the number of optimisation variables and a maximum number of 50 iterations is chosen as the stopping criteria. For the algorithm bounds, we let the total channel launch power vary between  $-10$  dBm and 25 dBm, and the power of each pump at the beginning of the fibre from 0 mW to 500 mW for the FW case, and from 0 mW to  $500 \cdot e^{-\alpha_p L}$  mW for the BW. At the end of the optimisation, we set 0 power for all the pumps with negligible

TABLE I  
PUMPS' POWER AND WAVELENGTH ALLOCATION WHICH YIELDS THE POWER PROFILES SHOWN IN FIG 5.

Wavelength [nm]	E-band								S-band	
	1388.2	1394.6	1401.2	1407.7	1427.9	1434.7	1441.6	1448.6	1477.1	1484.4
Forward Raman Pump Scenario										
FW pumps' power at $z = 0$ [mW]	16.3	47.4	50.4	44.7	64.2	-	435.7	132.5	500	-
Backward Raman Pump Scenario										
BW pumps' power at $z = L$ [mW]	9.5	-	-	-	-	83.8	-	-	-	1083.2
BW pumps' power at $z = 0$ [mW]	6.9	-	-	-	-	1.2	-	-	-	39.87

power at the beginning of the fibre for the FW case, and at the end of the fibre for BW case. For each one of the scenarios considered, the pumps' allocation with non-zero power found by the described algorithm is shown in Table I. For the FW-RA case, an optimum input launch power per channel of -3.9 dBm was found, resulting in a total launch power of 16.59 dBm, yielding to a total throughput of 201.67 Tbit/s. For the BW-RA case, an optimum input launch power per channel of -0.67 dBm was found, resulting in a total launch power of 19.82 dBm and yielding to a total throughput of 221.06 Tbit/s. The values obtained for the optimal spectrally uniform launch powers and the total throughput for each case are discussed and analysed in detail in the next sections.

Finally, note that the optimisation carried out in this section, may not necessarily be the optimum one, as more pumps could be considered in more wavelengths increasing the degrees of freedom, and also the optimisation bounds, chosen algorithm and algorithm setup could be changed to achieve better results. We chose the described setup for simplicity and to achieve real-time implementation of the PSO algorithm without requiring the utilisation of GPUs.

## VI. HYBRID-AMPLIFIER CHARACTERISATION

This section presents the characterisation of the Hybrid amplifier. To that end, for both the optimised scenarios described in Sec. V, we give the power profile evolution along the fibre distance, the hybrid amplifier gain, i.e., the distributed Raman on-off gain followed by the gain provided by the lumped amplifier placed at the end of the fibre. The results are shown for transmission after 1 span, as after 1 span the ASE noise from Raman and lumped amplifiers are not coupled yet (see Eq. (4)), so we can analyse its effects separately.

For the two scenarios described in Sec. V, the per-channel power profile along the distance, i.e., the solution of Eq. (2), are shown in Fig. 5 for (a) FW-RA and (b) BW-RA. It is interesting to note that, as shown in Eqs. (2) and (4), the intensity of Raman ASE noise, i.e. the noise generated before LA, is directly proportional to the intensity of the received launch power profiles. This means that for the FW-RA amplification, low levels of Raman ASE before LA are expected, however, higher NLI noise is generated given the higher power levels propagating along the fibre distance. In the case of BW-RA, the opposite effect happens. Higher ASE noise before LA is expected, however, lower NLI noise is also produced given the reduced power levels propagating along the fibre distance. Note that, for both cases, the Raman ASE noise is amplified by the lumped amplifier placed at the end of the span. These effects are quantified in detail in Sec. VII.

Fig. 6 shows the amplifier gain for hybrid (a) FW-RA and (b) BW-RA. The gains are shown for the optimised distributed Raman amplifier (red) and for the lumped amplifier (blue) placed at the end of each span. The total gain, i.e., the sum of the gain from the distributed Raman and lumped amplifier stages is also shown in green. This figure shows that most of the optimised amplifier gain comes from the distributed Raman stage. This is expected given the lower ASE generation by this kind of amplification technology when compared to the lumped ones. More interesting is the fact that a full Raman

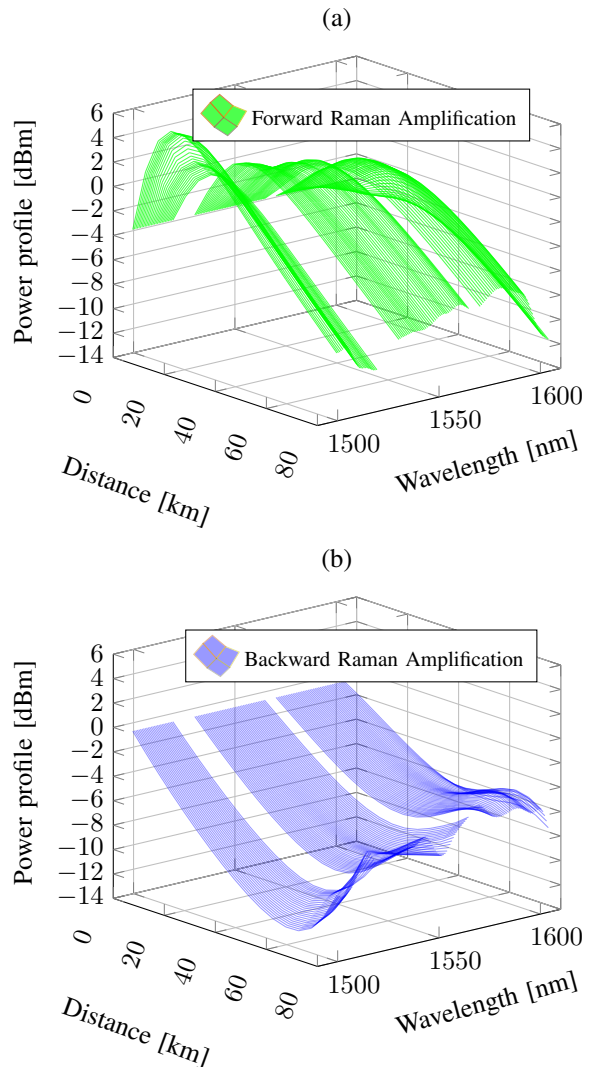


Fig. 5. Per-channel launch power evolution along the fibre distance for (a) FW-RA and (b) BW-RA.

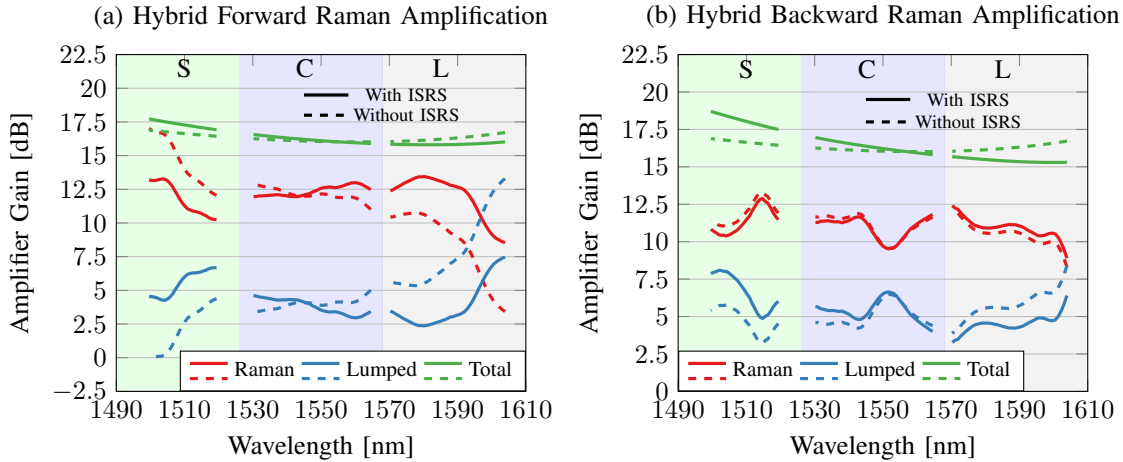


Fig. 6. Hybrid Amplifier gain designed in Sec. V for (a) FW-RA and (b) BW-RA. The gains for each one of the amplification stages are shown in red (RA stage) and blue (LA stage); the total gain is shown in green. The results are also computed with (continuous lines) and without (dashed lines) the ISRS effect.

gain, with no lumped amplifiers, might not be the best option, as, despite the greater performance of Raman amplifiers in terms of ASE generation, it may massively increase the NLI and ASE noise as a result of high pump powers.

In order to analyse the impact of ISRS effect, we also compute these gains in Fig. 6 with (continuous lines) and without (dashed lines) the ISRS effect. As expected for both scenarios, in the presence of ISRS more power is lost from the S-band towards the L-band, reducing the Raman amplifier gain in the lower-wavelength channels when compared to the higher ones. This reduction is then compensated by the ideal lumped amplifier, which gives more gain for channels located in the S-band. Note that, the total gain (green), corresponds to the fibre loss for the transmission without ISRS effect (dashed green lines), while the continuous green line represents the effect fibre loss (standard loss + ISRS effect), which is different for the hybrid FW and BW-RA schemes because each one of the systems has different values of total launch power (which changes the intensity of the ISRS effect); for the hybrid FW-RA case, the total optimised power is 16.59 dBm, while for the hybrid BW-RA case, this value is 19.82 dBm.

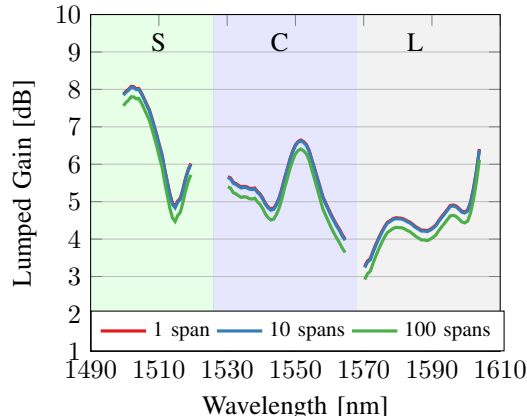


Fig. 7. Ideal gain from the lumped amplifiers placed at the end of the 1<sup>st</sup>, 10<sup>th</sup> and 100<sup>th</sup> span for the optimised hybrid BW-RA scenario.

As mentioned previously, the results shown in this section are computed after the first span. This is because the ASE noise from Raman and lumped amplifiers can be decoupled and the results can be presented separately for each one of the cases. It was also mentioned that the amplifier gain is not the same after each span because of the coupling between ASE noise and signal as per Eqs. (2) and 4, which results in the ASE noise affecting differently the signal and then, changing the on-off Raman gain and the ideal lumped gain provided by EDFAs and TDFAs after each span.

This change, however, is small and can be neglected as shown in Fig. 7. In this figure, the optimised hybrid BW-RA designed in Sec. V is used as an example, and the ideal gain from the lumped amplifier placed at the end of the 1<sup>st</sup>, 10<sup>th</sup> and 100<sup>th</sup> spans are shown. Because the ASE noise couples with the signal as shown in Eq. (2), the ideal lumped gain slightly reduces after each span. This change is less than 0.05 dB after 10 spans and less than 0.4 dB after 100 spans and thus can be neglected. This is effectively equivalent of assuming  $P_{\text{ASE}} = 0$  in Eq. (2). Because of that, the amplifier characteristics remain approximately unchanged for every span, and the gains presented in Fig 6 can also be assumed as the gain for the remaining spans with negligible errors.

## VII. SYSTEM PERFORMANCE FOR HYBRID-AMPLIFIED TRANSMISSION

This section shows the performance of the transmission systems considered in Secs. IV and V, for both optimised hybrid-amplified systems. The sources of noise, namely, ASE from the Raman amplifier, ASE from the lumped amplifier and NLI from the fibre transmission, are separated out and analysed for a single span. The total ASE and NLI noises are then computed for 10 and 100-span transmissions and a detailed discussion of the results is presented.

We start by separating and showing each one of the noise sources in Eq. (1). This is shown in Fig. 8 after 1 span transmission. As in the previous section, the choice of showing it for 1 span is based on the fact that this is the only scenario

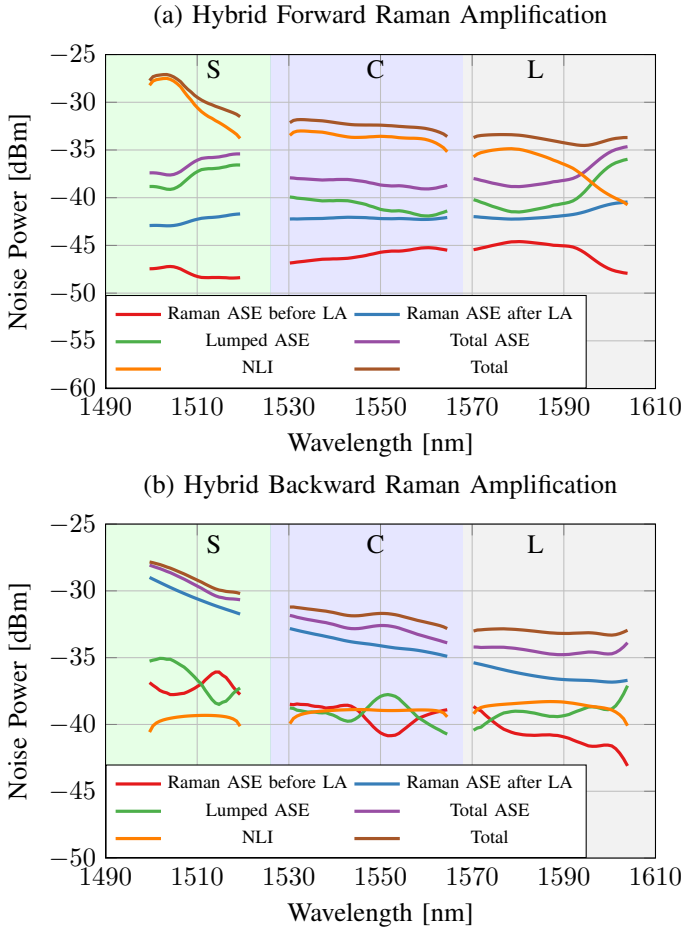


Fig. 8. Noise power contributions after the first span for hybrid (a) FW-RA and (b) BW-RA.

where we can separate the ASE noise generated from the Raman amplifier from that generated by LA. This is because after the first span, the total ASE noise (Raman + lumped) is used as the initial condition in Eq. (4), and thus, from the second span onwards both noises are coupled on the transmission and cannot be separated out.

Fig. 8 shows the different noise contributions from Eq. (1), for both hybrid amplifier schemes. The Raman ASE noise is shown before LA (red) and after being amplified by the ideal lumped amplified (blue) placed at the end of the span. The ASE noise from LA (green) obtained from Eq.(6) is also shown. The amplified Raman and the lumped ASE noise contributions are then summed and shown as the total ASE (purple). Finally, The NLI noise (orange), and the sum of the total ASE and NLI noises is shown as the total noise (brown). As already discussed previously, for (a) hybrid FW-RA, the ASE noise is lower and the NLI noise is higher which clearly shows that this system is NLI-noise limited. On the other hand, for (b) hybrid BW-RA, the ASE noise is the most impactful contribution while the NLI noise has a smaller contribution, showing that the system is ASE-noise limited. The explanation for this relies on the amount of power and ASE generated along the fibre transmission (see Fig. 5 and Sec. VI for a detailed explanation).

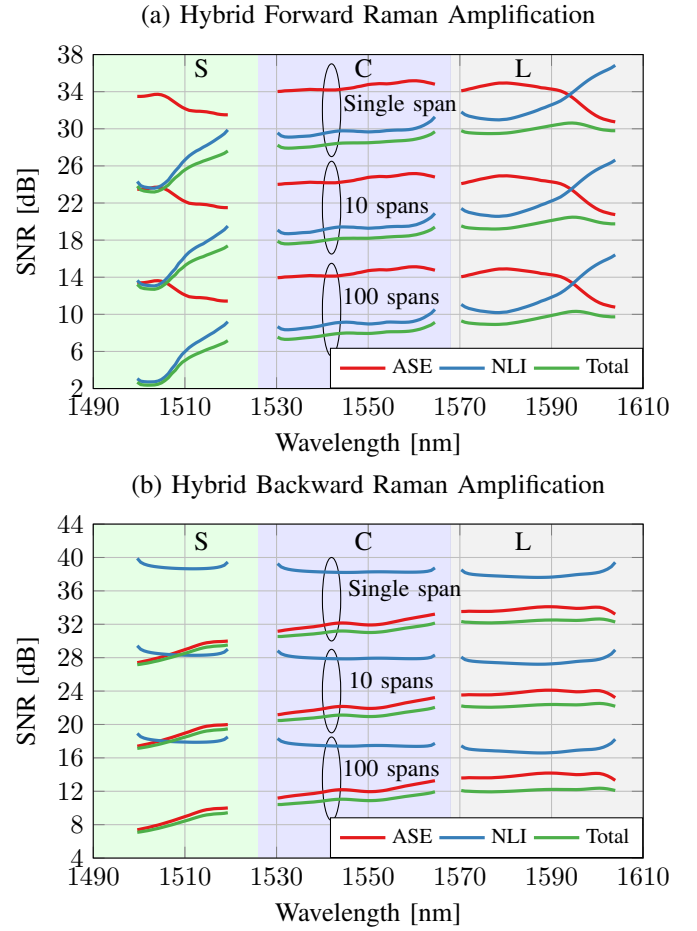


Fig. 9. SNR contributions after the 1<sup>st</sup>, 10<sup>th</sup> and 100<sup>th</sup> span for hybrid (a) FW-RA and (b) BW-RA.

Fig. 9 shows the different SNR contributions as a function of wavelength for the transmissions over 1, 10 and 100 spans for (a) FW-RA and (b) BW-RA. The ASE contribution corresponds to the total ASE noise generated by RA and LA. It is interesting to note the correlation of the SNR profile with the power profiles shown in Fig. 5. Indeed, for the hybrid-FW-RA case, shown in Fig. 9(a), the high-power levels in short wavelengths (see Fig. 5(a)) increases the NLI noise, reducing the SNR, degrading the performance of those channels; on the other hand, the performance of long-wavelength channels is higher, due to their reduced power levels, yielding to a tilt in the SNR profile. For the hybrid-BW-RA case, shown in Fig. 9(b) the increased received power levels in short wavelengths (see Fig. 5(b)) increases the ASE noise, reducing the SNR and degrading the performance of those channels; yielding to a similar tilt as the hybrid-FW-RA case. Once again for all the scenarios, it is possible to see the hybrid-FW-RA as an NLI-noise limited transmission system and the hybrid-BW-RA as an ASE-noise limited transmission system.

Note that, for all the results, the XPM generated by the pumps is neglected in the NLI noise calculation; as shown in [49], this is a valid assumption when the WDM spectra are sufficiently far from the pumps - in our case, as described in Secs. III and V, the highest-wavelength pump was chosen

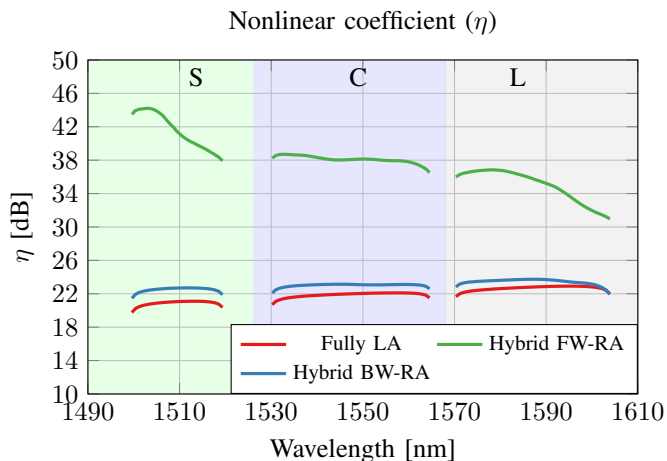


Fig. 10. Nonlinear coefficient after 1 span for the transmission system in Sec. IV for each amplification scheme.

to be 2 THz away from the lowest-wavelength channel, such that these effects could be neglected. Despite that, if needed, the aforementioned effects can be included in this model by considering the pumps as additional interfering channels.

### VIII. COMPARISON WITH FULLY LUMPED AMPLIFICATION

This section compares the transmission system described in Secs. IV and V with a fully lumped amplified link, i.e., without any pumps in the transmission fibre, such that the transmitted power is completely recovered with the ideal lumped amplifier placed at the end of each span. In order to simulate this transmission, the NLI model published in [45] was used with the same transmission setup described in Sec. IV. The results in terms of performance are then compared with those of Sec. VII and the differences are highlighted and discussed in detail.

The first step for carrying out this simulation was to consider a fully lumped transmission system with the same parameters as described in Sec. IV. As no pumps are placed in the transmission, we optimised only the total launch power of the system, which resulted in a total optimal launch power of 24.2 dBm, corresponding to 3.71 dBm per channel. This optimisation resulted in a total throughput of 177.73 Tbit/s over a single-span transmission.

Fig. 10 shows the nonlinear coefficient  $\eta$  (see Eq. (1)) obtained from each one of the amplification schemes, namely, hybrid FW-RA, hybrid BW-RA and fully LA. The motivation for plotting  $\eta$  is to analyse the amount of NLI noise generated by each amplification scheme if the launch power was the same for the optimised amplification schemes considered (this is because  $\eta$  only depends on the normalised launch power profile, and not on its absolute value). This figure shows that for the same launch power profile, the hybrid FW-RA generate higher amounts of NLI noise, because of its increased values of power propagating along the fibre distance (see Fig 5), while the LA case generates lower amounts of NLI noise (for the same launch power) because the power is just attenuated by the fibre loss and changed by the ISRS effect, i.e, no pumps are adding additional power in the fibre. Note that, in reality for the systems designed in this paper, because the launch power

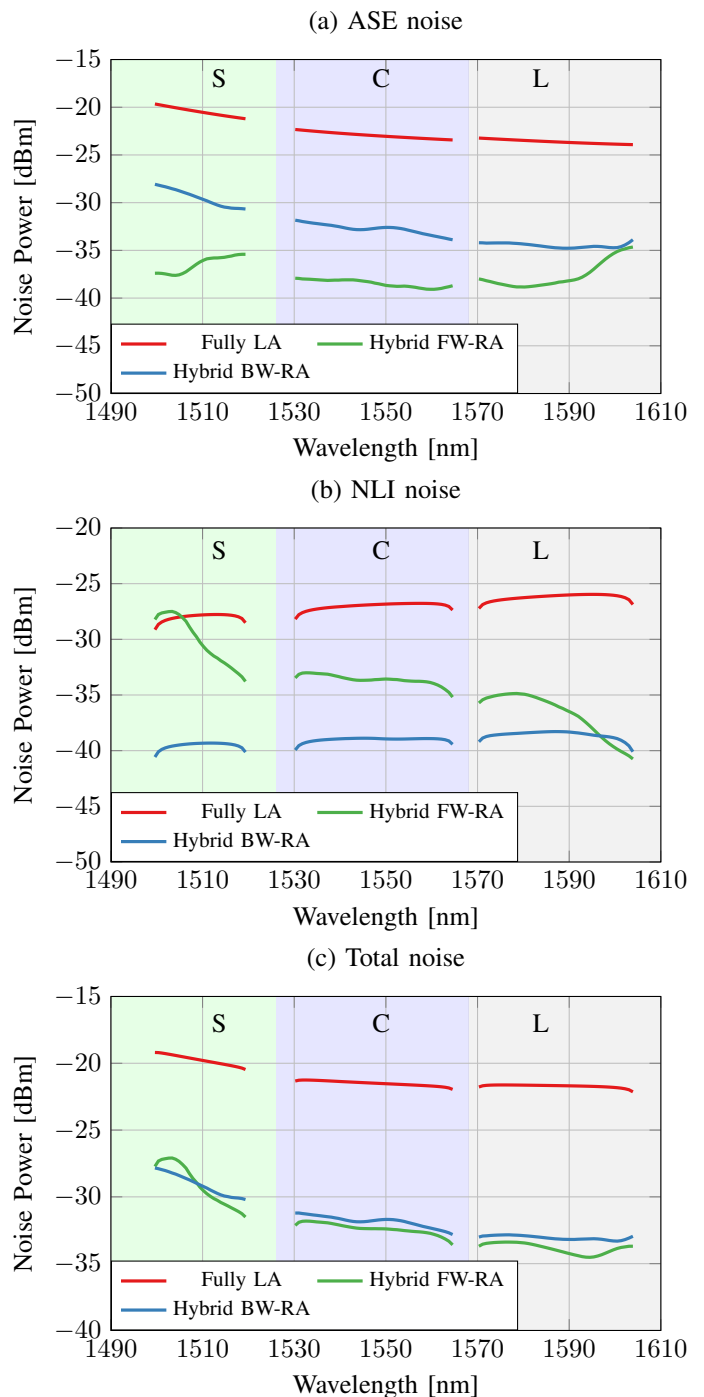


Fig. 11. Different noise power contributions after the 1<sup>st</sup> span for each amplification scheme.

is different for each amplification scheme and the NLI noise is proportional to this quantity to the power cube ( $P_{\text{NLI}} \propto P_i^3$ ), the absolute amount of NLI noise generated by each scheme depends on the launch power. Indeed, the higher launch power for the fully LA scenario (24.2 dBm) makes this case the worst performing case in terms of NLI noise generation as shown in Fig. 11.(b).

Fig. 11 shows the different noise contributions for each one of the amplification schemes designed in this work. Fig. 11.(a)

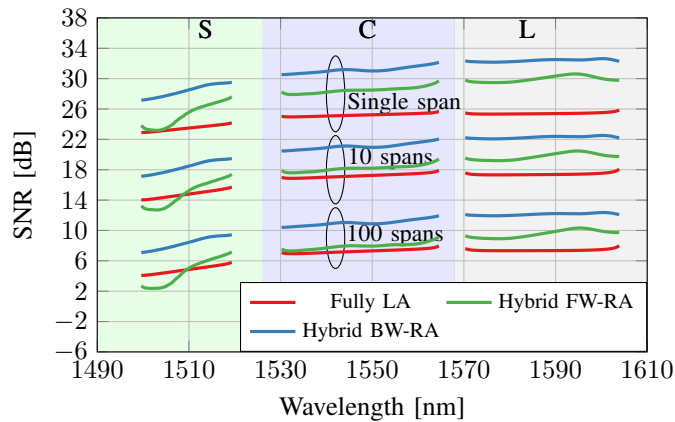


Fig. 12. Total SNR contribution after the 1<sup>st</sup>, 10<sup>th</sup> and 100<sup>th</sup> span for each amplification scheme.

shows that the LA case presents higher ASE noise generation, which motivates the utilisation of hybrid amplifiers to achieve higher throughput. Fig. 11.(b), shows that because of the increased total launch power of the LA case (24.2 dBm) it also generates higher amounts of NLI noise, with its performance better than the FW-RA case in the lower-wavelength channels of the S-band, even with this latter amplification scheme having the lowest total launch power (16.59 dBm). Finally, Fig. 11.(c), shows that, overall, LA is the worst-case scenario in terms of noise generation, followed by the hybrid BW-RA and FW-RA. This is not an indication of which amplification scheme is better as the SNR calculation also depends on the launch power.

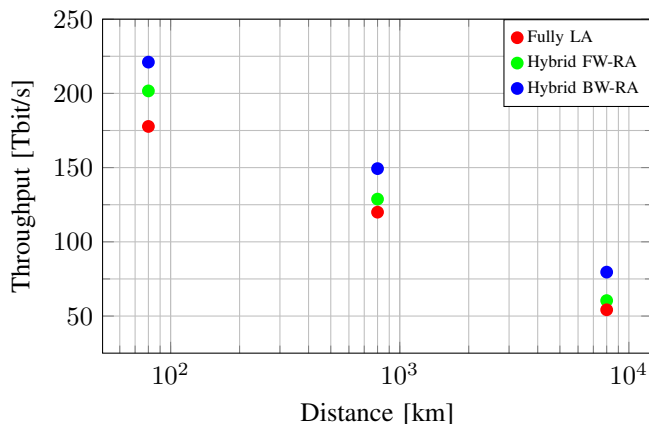


Fig. 13. Total throughput achieved by the different amplification schemes after 1, 10 and 100 spans.

In order to analyse which is the best amplification scheme, Fig.12 shows the total SNR contributions for the transmission over 1, 10 and 100 spans for each one of the designed amplifiers. This figure shows that the hybrid BW-RA presents the best compromise between launch power, ASE and NLI noise, achieving the best performance. The worst performance is obtained by the fully lumped case, which is mainly a result of the bad ASE performance. Note that the FW-RA is the worst-performing scheme for lower-wavelength channels

placed at the S-band - this is because of the high amounts of NLI noise generated by the hybrid FW-RA case for channels located in that band. Finally, the results presented in Fig.12 are also shown in terms of total throughput in Fig. 13.

Fig. 13 shows the total throughput achieved by each one of the amplification schemes by using Eq. (12). For transmission over a single span, the throughput obtained are 221.06 Tbit/s, 201.67 Tbit/s, and 177.73 Tbit/s, respectively for the hybrid BW-RA, hybrid FW-RA and LA. For the transmission after 10 spans these values are respectively 149.32 Tbit/s, 128.77 Tbit/s, and 119.98 Tbit/s. Finally, for the transmission over 100 spans, these values are respectively 79.59 Tbit/s, 60.41 Tbit/s, and 54.22 Tbit/s. It is interesting to note how the total throughput for hybrid FW-RA approximates that of the LA for long distances. This is because the optimisation performed in Sec. V was done for a single span. The same optimisation done for 10 or 100 spans would yield different results increasing the performance of both hybrid FW-RA and BW-RA amplification schemes.

## IX. CONCLUSIONS

In this work, we present the first fully analytical model to evaluate an optical fibre transmission system using hybrid amplification. This analytical model is the first capable of accounting for any setup of Raman amplification technology, such as any number of pumps, forward and backward pumping configurations, wavelength-dependent fibre parameters, different bandwidth per channel, any modulation format and arbitrary per-channel launch power values, including non-uniform launch power profiles. This model includes the estimation of fibre nonlinear interference and the spontaneous emission noise generated by Raman amplified links. The TRX impairment is also included.

The model is capable of accurately estimating the optical system performance after an arbitrary number of spans, being suitable for real-time estimation, optimisation routines and fast optical transmission performance analysis. Because of the speed of computation, the formula can also be applied as an enabling tool for future intelligent and dynamic optical fibre networks. The model is an approximation in closed-form formula from the Gaussian noise model and is used in this paper for several analyses of hybrid amplified optical links, where distributed Raman amplification is used in combination with lumped amplifiers.

The model is suitable for ultra-wideband fibre transmission, as it supports the ISRS effect together with Raman amplification. The analysis in this work is done over an optical transmission system with 13 THz (105 nm) of optical signal, corresponding to the utilisation of the S-, C- and L-bands. The effects of ISRS and Raman amplification and their implications in the signal and in the system performance are discussed and analysed.

Scenarios ranging from short to metro, long-haul and trans-Atlantic transmission systems are considered. For these scenarios, the best hybrid Raman amplifier is designed based on a particle swarm optimisation algorithm, where the best pumps' wavelengths and powers are calculated to maximise the total

system throughput of a multi-span system over 80 km standard single-mode fibre. Launch power optimisation is also carried out to maximise the performance.

For the optimised hybrid amplifiers, their full characterisation in terms of gain is presented. Moreover, all the sources of noise are analysed in detail, and their relation with the performance of the optical fibre amplifier technology chosen is also assessed. A comparison with an optimised fully lumped amplifier is presented showing how hybrid amplifiers are able to outperform EDFAs and TDFAs. This work also shows how to design high-capacity achieving hybrid amplifiers using analytical modelling.

Among the several results of this paper, we design a hybrid backward Raman amplifier achieving 221.06 Tbit/s over a single 80 km span transmission, and a hybrid forward Raman amplifier achieving 201.67 Tbit/s over the same system. In comparison, a fully lumped optimised amplifier is shown to achieve no more than 177.73 Tbit/s in the same conditions.

## REFERENCES

- [1] R.J. Mears, L. Reekie, I.M. Jauncey, and D.N. Payne, "Low-noise erbium-doped fibre amplifier operating at 1.54  $\mu$  m," *Electronics Letters*, vol. 23, no. 19, pp. 1026 – 1028, 1987.
- [2] Takeshi Hoshida, Vittorio Curri, Lidia Galdino, David T. Neilson, Wladek Forsyia, Johannes K. Fischer, Tomoyuki Kato, and Pierluigi Poggiolini, "Ultrawideband systems and networks: beyond C + L-band," *Proceedings of the IEEE*, vol. 110, no. 11, pp. 1725–1741, 2022.
- [3] Henrique Buglia, Eric Sillekens, Anastasiia Vasylychenkova, Wenting Yi, Robert Killey, Polina Bayvel, and Lidia Galdino, "Challenges in extending optical fibre transmission bandwidth beyond C+L band and how to get there," in *2021 International Conference on Optical Network Design and Modeling (ONDM)*, 2021.
- [4] H. Buglia, E. Sillekens, A. Vasylychenkova, P. Bayvel, and L. Galdino, "On the impact of launch power optimization and transceiver noise on the performance of ultra-wideband transmission systems [invited]," *Journal of Optical Communications and Networking*, vol. 14, no. 5, pp. B11–B21, 2022.
- [5] Benjamin J. Puttnam, Ruben S. Luis, Georg Rademacher, Yoshinari Awaji, and Hideaki Furukawa, "Investigation of long-haul S-, C- + L-band transmission," in *2022 Optical Fiber Communications Conference and Exhibition (OFC)*, 2022.
- [6] J. . Cai, H. G. Batshon, M. V. Mazurczyk, C. R. Davidson, O. V. Sinkin, D. Wang, M. Paskov, W. W. Patterson, M. A. Bolshtyansky, and D. G. Foursa, "94.9 Tb/s single mode capacity demonstration over 1,900 km with C+L EDFAs and coded modulation," in *European Conference on Optical Communication (ECOC)*, 2018.
- [7] J. . Cai, H. G. Batshon, M. V. Mazurczyk, O. V. Sinkin, D. Wang, M. Paskov, W. Patterson, C. R. Davidson, P. Corbett, G. Wolter, T. Hammon, M. Bolshtyansky, D. Foursa, and A. Pilipetskii, "70.4 Tb/s capacity over 7,600 km in C+L band using coded modulation with hybrid constellation shaping and nonlinearity compensation," in *Optical Fiber Communications Conference (OFC)*, 2017.
- [8] J. Cai, Y. Sun, H. Zhang, H. G. Batshon, M. V. Mazurczyk, O. V. Sinkin, D. G. Foursa, and A. Pilipetskii, "49.3 Tb/s transmission over 9100 km using C+L EDFA and 54 Tb/s transmission over 9150 km using hybrid-Raman EDFA," *Journal of Lightwave Technology*, vol. 33, no. 13, pp. 2724–2734, 2015.
- [9] J. Cai, H. G. Batshon, M. V. Mazurczyk, O. V. Sinkin, D. Wang, M. Paskov, C. R. Davidson, W. W. Patterson, A. Turukhin, M. A. Bolshtyansky, and D. G. Foursa, "51.5 Tb/s capacity over 17,107 km in C+L bandwidth using single-mode fibers and nonlinearity compensation," *Journal of Lightwave Technology*, vol. 36, no. 11, pp. 2135–2141, 2018.
- [10] L. Galdino, D. Semrau, M. Ionescu, A. Edwards, W. Pelouch, S. Desbruslais, J. James, E. Sillekens, D. Lavery, S. Barnes, R. I. Killey, and P. Bayvel, "Study on the impact of nonlinearity and noise on the performance of high-capacity broadband hybrid Raman-EDFA amplified system," *Journal of Lightwave Technology*, vol. 37, no. 21, pp. 5507–5515, 2019.
- [11] M. Ionescu, D. Lavery, A. Edwards, E. Sillekens, D. Semrau, L. Galdino, R. I. Killey, W. Pelouch, S. Barnes, and P. Bayvel, "74.38 Tb/s transmission over 6300 km single mode fibre enabled by C+L amplification and geometrically shaped PDM-64QAM," *Journal of Lightwave Technology*, vol. 38, no. 2, pp. 531–537, 2020.
- [12] J. Renaudier, A. Arnould, D. Le Gac, A. Ghazisaeidi, P. Brindel, M. Makhsiyani, A. Verdier, K. Mekhazni, F. Blache, H. Debregeas, A. Boutin, N. Fontaine, D. Neilson, R. Ryf, H. Chen, M. Achouche, and G. Charlet, "107 Tb/s transmission of 103-nm bandwidth over 3x100 km SSMF using ultra-wideband hybrid Raman/SOA repeaters," *Optical Fiber Communication Conference (OFC)*, p. Tu3F.2, 2019.
- [13] Amirhossein Ghazisaeidi, Aymeric Arnould, Maria Ionescu, Vahid Aref, Haik Mardoyan, Sophie Etienne, Mathieu Duval, Christian Bastide, Hans Bissessur, and Jeremie Renaudier, "99.35 tb/s ultra-wideband unrepeatable transmission over 257 km using semiconductor optical amplifiers and distributed Raman amplification," *Journal of Lightwave Technology*, vol. 40, no. 21, pp. 7014–7019, 2022.
- [14] Xiaohui Zhao and et. al, "200.5 Tb/s transmission with S+C+L amplification covering 150 nm bandwidth over 2x100 km PSCF spans," *2022 European Conference on Optical Communication (ECOC)*, p. Th3C.4, 2022.
- [15] J. Renaudier, A. C. Meseguer, A. Ghazisaeidi, P. Tran, R. R. Muller, R. Brenot, A. Verdier, F. Blache, K. Mekhazni, B. Duval, H. Debregeas, M. Achouche, A. Boutin, F. Morin, L. Letteron, N. Fontaine, Y. Frignac, and G. Charlet, "First 100-nm continuous-band WDM transmission system with 115Tb/s transport over 100km using novel ultra-wideband semiconductor optical amplifiers," in *European Conference on Optical Communication (ECOC)*, 2017.
- [16] Fukutaro Hamaoka, Masanori Nakamura, Seiji Okamoto, Kyo Minoguchi, Takeo Sasai, Asuka Matsushita, Etsushi Yamazaki, and Yoshiaki Kisaka, "Ultra-wideband WDM transmission in S-, C-, and L-bands using signal power optimization scheme," *Journal of Lightwave Technology*, vol. 37, no. 8, pp. 1764–1771, 2019.
- [17] Lidia Galdino, Adrian Edwards, Wenting Yi, Eric Sillekens, Yuta Wakayama, Thomas Gerard, Wayne Sheldon Pelouch, Stuart Barnes, Takehiro Tsuritani, Robert I Killey, et al., "Optical fibre capacity optimisation via continuous bandwidth amplification and geometric shaping," *IEEE Photonics Technology Letters*, vol. 32, no. 17, pp. 1021–1024, 2020.
- [18] Benjamin J. Puttnam, Ruben S. Luis, Georg Rademacher, Manuel Mendez-Astudilio, Yoshinari Awaji, and Hideaki Furukawa, "S-, C- and extended L-band transmission with doped fiber and distributed Raman amplification," *Optical Fiber Communication Conference (OFC)*, p. Th4C.2, 2021.
- [19] Benjamin J. Puttnam, Ruben S. Luis, Georg Rademacher, Manuel Mendez-Astudilio, Yoshinari Awaji, and Hideaki Furukawa, "S-, C- and L-band transmission over a 157nm bandwidth using doped fiber and distributed Raman amplification," *Opt. Express*, vol. 30, no. 6, pp. 10011–10018, Mar 2022.
- [20] André Souza, Nelson Costa, Jo ao Pedro, and Jo ao Pires, "Benefits of counterpropagating Raman amplification for multiband optical networks," *J. Opt. Commun. Netw.*, vol. 14, no. 7, pp. 562–571, Jul 2022.
- [21] Robin Matzner, Daniel Semrau, Ruijie Luo, Georgios Zervas, and Polina Bayvel, "Making intelligent topology design choices: understanding structural and physical property performance implications in optical networks," *Journal of Optical Communications and Networking*, vol. 13, no. 8, pp. D53–D67, Aug 2021.
- [22] Ruijie Luo, Robin Matzner, Alessandro Ottino, Georgios Zervas, and Polina Bayvel, "Exploring the relationship among traffic, topology, and throughput: towards a traffic-optimal optical network topology design," *Journal of Optical Communications and Networking*, vol. 15, no. 5, pp. B1–B10, May 2023.
- [23] Pierluigi Poggiolini, "The GN model of non-linear propagation in uncompensated coherent optical systems," *Journal of Lightwave Technology*, vol. 30, no. 24, pp. 3857–3879, 2012.
- [24] Andrea Carena, Gabriella Bosco, Vittorio Curri, Yanchao Jiang, Pierluigi Poggiolini, and Fabrizio Forghieri, "EGN model of non-linear fiber propagation," *Opt. Express*, vol. 22, no. 13, pp. 16335–16362, Jun 2014.
- [25] Daniel Semrau, Robert I. Killey, and Polina Bayvel, "The Gaussian noise model in the presence of inter-channel stimulated Raman scattering," *Journal of Lightwave Technology*, vol. 36, no. 14, pp. 3046–3055, 2018.
- [26] Gabriella Bosco, "Complexity versus accuracy tradeoffs in nonlinear fiber propagation models," *Optical Fiber Conference (OFC)*, 2023.
- [27] P. Poggiolini, M. Ranjbar Zefreh, G. Bosco, F. Forghieri, and S. Piciaccia, "Accurate non-linearity fully-closed-form formula based on the GN/EGN model and large-data-set fitting," in *2019 Optical Fiber Communications Conference and Exhibition (OFC)*, 2019, pp. 1–3.

- [28] Daniel Semrau, Robert I. Killey, and Polina Bayvel, "A closed-form approximation of the Gaussian noise model in the presence of inter-channel stimulated Raman scattering," *Journal of Lightwave Technology*, vol. 37, no. 9, pp. 1924–1936, 2019.
- [29] Mahdi Ranjbar Zefreh, Fabrizio Forghieri, Stefano Piciaccia, and Pierluigi Poggiolini, "Accurate closed-form real-time EGN model formula leveraging machine-learning over 8500 thoroughly randomized full C-band systems," *Journal of Lightwave Technology*, vol. 38, no. 18, pp. 4987–4999, 2020.
- [30] Daniel Semrau, Eric Sillekens, Robert I. Killey, and Polina Bayvel, "A modulation format correction formula for the Gaussian noise model in the presence of inter-channel stimulated Raman scattering," *Journal of Lightwave Technology*, vol. 37, no. 19, pp. 5122–5131, 2019.
- [31] Mahdi Ranjbar Zefreh and Pierluigi Poggiolini, "A real-time closed-form model for nonlinearity modeling in ultra-wide-band optical fiber links accounting for inter-channel stimulated Raman scattering and co-propagating Raman amplification," 2020.
- [32] M. Ranjbar Zefreh, F. Forghieri, S. Piciaccia, and P. Poggiolini, "A closed-form nonlinearity model for forward-Raman-amplified WDM optical links," in *Optical Fiber Communication Conference (OFC) 2021*, 2021, p. M5C.1, Optica Publishing Group.
- [33] Pierluigi Poggiolini and Mahdi Ranjbar-Zefreh, "Closed form expressions of the nonlinear interference for UWB systems," in *2022 European Conference on Optical Communication (ECOC)*, 2022.
- [34] H. Buglia, E. Sillekens, A. Vasylenkova, R.I. Killey, P. Bayvel, and L. Galdino, "An extended version of the ISRS GN model in closed-form accounting for short span lengths and low losses," in *2022 European Conference on Optical Communication (ECOC)*, 2022.
- [35] H. Buglia, M. Jarmolovičius, A. Vasylenkova, E. Sillekens, L. Galdino, R. I. Killey, and P. Bayvel, "A closed-form expression for the Gaussian noise model in the presence of inter-channel stimulated Raman scattering extended for arbitrary loss and fibre length," *Journal of Lightwave Technology*, pp. 1–10, 2023.
- [36] Daniel Semrau, Gabriel Saavedra, Domaniç Lavery, Robert I. Killey, and Polina Bayvel, "A closed-form expression to evaluate nonlinear interference in Raman-amplified links," *Journal of Lightwave Technology*, vol. 35, no. 19, pp. 4316–4328, 2017.
- [37] Henrique Buglia, Mindaugas Jarmolovicius, Anastasiia Vasylenkova, Eric Sillekens, Lidia Galdino, Polina Bayvel, and Robert Killey, "A closed-form expression for the ISRS GN model supporting distributed Raman amplification," *Optical Fiber Conference (OFC)*, 2023.
- [38] H. Buglia, M. Jarmolovicius, L. Galdino, R. I. Killey, and P. Bayvel, "A closed-form expression for the Gaussian noise model in the presence of Raman amplification," *arXiv:2304.11974 [eess.SP]*, 2023.
- [39] H. Buglia, M. Jarmolovicius, L. Galdino, R. I. Killey, and P. Bayvel, "A modulation-format dependent closed-form expression for the Gaussian noise model in the presence of Raman amplification," *European Conference on Optical Communication (ECOC)*, 2023.
- [40] Ian Roberts, Joseph M Kahn, James Harley, and David W Boertjes, "Channel power optimization of WDM systems following Gaussian noise nonlinearity model in presence of stimulated Raman scattering," *Journal of Lightwave Technology*, vol. 35, no. 23, pp. 5237–5249, 2017.
- [41] Sam Nallaperuma, Nikita A. Shevchenko, and Seb J. Savory, "Parameter optimisation for ultra-wideband optical networks in the presence of stimulated Raman scattering effect," in *International Conference on Optical Network Design and Modeling (ONDM)*, 2021.
- [42] Bruno Correia, Rasoul Sadeghi, Emanuele Virgillito, Antonio Napoli, Nelson Costa, João Pedro, and Vittorio Curri, "Optical power control strategies for optimized C+L+S-bands network performance," in *Optical Fiber Communications Conference*, 2021.
- [43] A. M. Rosa Brusin, M. Ranjbar Zefreh, P. Poggiolini, S. Piciaccia, F. Forghieri, and A. Carena, "Machine learning for power profiles prediction in presence of inter-channel stimulated Raman scattering," in *European Conference on Optical Communication (ECOC)*, 2021.
- [44] Bruno Correia, Rasoul Sadeghi, Emanuele Virgillito, Antonio Napoli, Nelson Costa, Joao Pedro, and Vittorio Curri, "Power control strategies and network performance assessment for C+L+S multiband optical transport," *Journal of Optical Communications and Networking*, vol. 13, no. 7, pp. 147–157, 2021.
- [45] Daniel Semrau, Robert I. Killey, and Polina Bayvel, "A closed-form approximation of the Gaussian noise model in the presence of inter-channel stimulated Raman scattering," *Journal of Lightwave Technology*, vol. 37, no. 9, pp. 1924–1936, 2019.
- [46] Pierluigi Poggiolini, "A generalized GN-model closed-form formula," *arXiv: 1810.06545 [eess.SP]*, 2018.
- [47] Uiara C. de Moura, Francesco Da Ros, A. Margareth Rosa Brusin, Andrea Carena, and Darko Zibar, "Experimental characterization of Raman amplifier optimization through inverse system design," *Journal of Lightwave Technology*, vol. 39, no. 4, pp. 1162–1170, 2021.
- [48] M Soltani, F Da Ros, A Carena, and D Zibar, "Distance and spectral power profile shaping using machine learning enabled Raman amplifiers," in *IEEE Photonics Society Summer Topicals Meeting Series (SUM)*, 2021.
- [49] Md Asif Iqbal, Gabriele Di Rosa, Lukasz Krzaczanowicz, Ian Phillips, Paul Harper, André Richter, and Wlodek Forysiak, "Impact of pump-signal overlap in S+C+L band discrete Raman amplifiers," *Opt. Express*, vol. 28, no. 12, pp. 18440–18448, Jun 2020.
- [50] J. Kennedy and R. Eberhart, "Particle swarm optimization," *Proceedings of ICNN'95 - International Conference on Neural Networks*, vol. 4, pp. 1942–1948, 1995.